



Mathematical modeling and numerical characterization of composite thermoelectric devices

B.V.K. Reddy*, Matthew Barry, John Li, Minking K. Chyu

Department of Mechanical Engineering and Materials Science, University of Pittsburgh, Pittsburgh, PA 15261, USA

ARTICLE INFO

Article history:

Received 4 March 2012

Received in revised form

13 September 2012

Accepted 15 November 2012

Available online 4 January 2013

Keywords:

Thermoelectrics

Composite

Conventional

Waste heat recovery

Performance

Numerical model

ABSTRACT

A Composite Thermoelectric Device (CTED) is comprised of thermoelectric (TE) elements made of TE semiconductor materials bonded to highly electrically and thermally conductive material in a segmented fashion. Thermoelectric performance of such devices using numerical methods with temperature-dependent thermoelectrical properties has been investigated. The CTED performance in terms of produced electrical current, Ohmic and Seebeck potentials, power output P_0 , heat input Q_h , and conversion efficiency η is studied for various hot surface temperature T_h , load resistance, semiconductor thickness d , and convection heat transfer coefficient h values. The aforementioned CTED performance characteristics are compared to those of a conventional TED with geometrical equivalence. For a given T_h , a maximum P_0 is achieved at a load resistance value that is equal to the total internal resistance R_i of the device; an optimum η , at an optimum load resistance R_{optml} which is typically higher than the R_i . A CTED with $d = 1$ mm, the optimum η values are 24.8%, 26.2% and 29.9% higher than conventional TED values at $T_h = 350$ K, 450 K and 550 K, respectively. At R_{optml} values, the difference in P_0 and Q_h show significant and minor increases, respectively, in relation to differences in η with an increase in T_h . The variation of the semiconductor thickness d has a substantial effect on the CTED characteristics and R_{optml} values; as d decreases, a continuous increase in P_0 and Q_h and an optimum value of η are achieved. Intuitively, R_{optml} increases with an increase in d and it reaches a maximum value at the conventional TED limit. With $d = 0.5$ mm, $T_h = 450$ K and $h = 20 \text{ W m}^{-2} \text{ K}^{-1}$ at a corresponding R_{optml} value, P_0 and Q_h exhibit an eight- and six-fold increase, respectively, and η is increased 22% compared to a conventional TED. The convective heat transfer coefficient has a pronounced effect on the CTED performance when it is greater than $100 \text{ W m}^{-2} \text{ K}^{-1}$. From this study, the CTEDs show promise of extracting more heat in waste heat recovery applications when compared to conventional TEDs.

© 2012 Elsevier Masson SAS. All rights reserved.

1. Introduction

Approximately two-thirds of the fossil-fuel energy we use in automobiles, power plants, and industrial systems is rejected into the atmosphere as waste heat. A viable technology for efficiently converting waste heat into electricity is thermoelectric devices (TEDs). Based on the principle of Seebeck effect, these devices work as a power generators by maintaining a temperature difference between hot and cold junctions. They have no moving parts, emit no noise and are environmental friendly.

Over the past few decades, TEDs made of bulk bismuth–antimony–telluride–selenium (Bi, Sb, Te, Se) have not shown an

increase in either their performance (Figures of Merit ($ZT \approx 1$) or thermal conversion efficiencies ($\approx 5\text{--}10\%$) [1,2]. However, with the growing environmental consciousness, there is a renewed interest in enhancing these renewable and sustainable device's performance for electrical power generation and waste heat recovery applications (up to $\approx 30\%$) via methods of nano-structuring, nano-fabrication and use of new bulk materials [3]. Caillat et al. [4] developed a segmented TED which operates over a temperature range of 300–973 K using novel p-type ($\text{Zn}_4\text{Sb}_3\text{CeFe}_4\text{Sb}_{14}$) and n-type (CoSb_3) based alloys. They achieved a conversion efficiency of 15% and also demonstrated the bonding studies between the segments. Gou et al. [5] investigated the performance of low temperature waste heat recovery TEDs using one-dimensional (1D) numerical simulations and experiments. They concluded that in addition to increasing the waste heat temperature and number of modules in series, expanding the heat sink surface area and enhancing the cold side heat transfer in proper ranges can have

* Corresponding author. Tel.: +1 412 624 9720; fax: +1 412 624 4846.

E-mail addresses: bvkreddy680@gmail.com (B.V.K. Reddy), matthew.michael.barry@gmail.com (M. Barry), johnli407@yahoo.com (J. Li), mkchu@pitt.edu (M.K. Chyu).

Nomenclature	
A	cross-sectional area, mm ²
A_s	surface area, mm ²
d	semiconductor thickness, mm
D	depth, mm
h	convection heat transfer coefficient, W m ⁻² K ⁻¹
H	height, mm
I	electric current, A
J	electric current density, A m ⁻²
\mathbf{J}	electric current density, vector
L	length, mm
P_0	power output ($I^2 R_L$), W
q''	heat flux, W m ⁻²
Q	heat transfer, W
T	temperature, K
V	voltage, V
R	electric resistance, Ω
W	width, mm
<i>Greek symbols</i>	
α	Seebeck coefficient or thermopower, V K ⁻¹
ε	emissivity, dimensionless
η	thermal efficiency, dimensionless
κ	thermal conductivity, W m ⁻¹ K ⁻¹
ρ	electrical resistivity, Ω m
σ	Boltzmann constant, W m ² K ⁴
<i>Subscripts</i>	
c	cold wall, conductor
i	internal
ic	inter-connector
h	hot wall
L	load
n	n-type semiconductor
$optmL$	optimum load
O	Ohmic
p	p-type semiconductor
S	Seebeck
sur	surroundings
ξ	normal surface
∞	ambient

dramatic effects on TED's performance. Furthermore, Hsiao et al. [6] also developed a 1D thermal resistance model for thermoelectric modules with applications to waste heat recovery from an automobile engine and compared their model results with experimental data. Their outcomes showed that the thermoelectric module on the exhaust pipe performs better compared to a module on the radiator system.

Most of the studies in literature were investigated with 1D models, even though electric field and temperature distributions are multidimensional in TEDs. Moreover, the heat flux and current density are not in parallel in conventional TEDs. Therefore, considering the three-dimensional (3D) effects in numerical models will give more realistic characteristics of TED performance. It has been shown in the articles [7–15] that 3D simulations are more accurate in design and optimization of TEDs. They conducted numerical simulations of TEDs with in-house codes as well as with available commercial software packages. Harris et al. [7] developed a finite volume based numerical code with temperature-dependent material properties to study 3D temperature and electrical field distributions in TEDs. They investigated the device performance by taking into consideration both thermal and electrical contact resistances at the interfaces of the thermoelectric material and conducting shoes. Additionally, they analyzed the TED with inert gas and insulating materials between element legs, to reduce and eliminate convection between hot and cold surfaces within said device, respectively. Chen et al. [8] analyzed the thermoelectric generator performance connected to various models of load circuitry in a SPICE-package environment and validated their results with ANSYS and experimental results. Further, Hu [9] studied the characteristics of two compact gas-phase heat exchangers placed on the hot and cold sides of the TED to enhance heat transfer and fluid flow while minimizing thermal stresses.

Ziólkowski et al. [10] analyzed the performance of thermoelectric generators including the parasitic effects such as convection, radiation and conduction heat bypass. They also considered the design parameters such as pellet aspect ratios and thermal and electrical contact resistances. Kousksou et al. [11] examined the thermoelectric power generation from a helicopter conical nozzle.

They showed that the electric power produced is sensitive to the hot fluid properties and significantly depends on actual operating conditions. Using Technology Computer-Aided Design (TCAD) package, Gould et al. [12] simulated the thermoelectric couple configured for low power generation. Chen et al. [13] proposed and implemented a 3D numerical model for thermoelectric generators in FLUENT UDS (User Defined Scalar) environment. This model accounts for all temperature-dependent properties of materials and non-linear fluid-thermal-electric multiphysics coupled effects. The model was validated with simulation data from other models and experimental data. Recently, in the articles [14–16], using 3D numerical methods implemented in FLUENT UDS package and analytical solutions, the authors studied the enhanced heat transfer characteristics and performance of composite and integrated TEDs applied to waste heat recovery systems. Further, various researchers studied optimum geometric dimensions to achieve maximum conversion efficiency of TEDs [17,18].

A review of literature suggests there is increasing interest in advanced TE materials research for higher ZT and the exploration of novel TED designs for increased performance while promoting the notion of sustainability. State-of-the-art and sustainable TED designs constructed with minimum amounts of rare-earth material without compromising conversion efficiency and performance while increasing the power output is one of the methods to minimize the device's cost. A potential and promising approach is to use a novel composite thermoelectric device (CTED), where a major part of the semiconductor is replaced with a conductor such as copper. In this work, by concentrating on the structuring of bulk materials, the performance of CTEDs compared with conventional TEDs has been investigated using a 3D numerical model implemented in the FLUENT UDS environment.

2. Geometry, mathematical model and boundary conditions

The three-dimensional schematics of composite and conventional thermoelectric devices (TEDs) being investigated are shown in Fig. 1a and b, respectively. The TED consists of two vertical legs connected electrically in series and thermally in parallel via

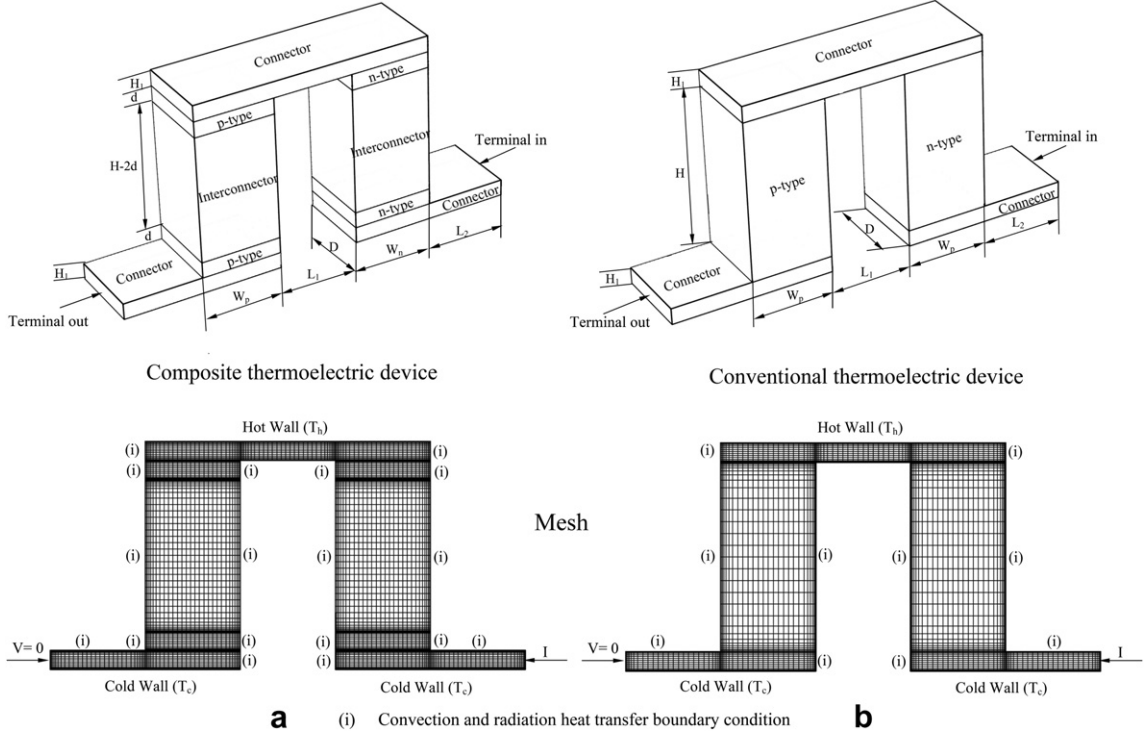


Fig. 1. Schematic of (a) composite and (b) convective thermoelectric devices.

connectors made of a highly electrical conducting material. The composite TED (CTED) leg consists of a copper inter-connector interposed between bulk crystalline n-type or p-type materials, whereas a convectional TED leg is entirely made of either n-type or p-type material. The semiconductor thickness d has been taken equal in size for both the left and right legs of the CTED. Each leg has a square cross-section $W \times D$ and height H , and the legs are separated by a distance L_1 as shown in Fig. 1. The top and bottom surface of each leg are connected to copper connectors. The end surfaces of these connectors act as electric terminals for load circuitry of load resistance (R_L). The top surface of the upper connector is subjected to constant hot temperature (T_h) while the bottom surface of the lower connector is maintained at a constant cold temperature (T_c). The remaining surfaces of connector, n-type, p-type, and inter-connector (exposed to ambient as shown in Fig. 1, marked with (i)) are subjected to convection and radiation heat transfer boundary conditions.

In the thermoelectric material, the current flow and energy transport are governed by the continuity of current density and the energy equations subjected to following assumptions: the

materials are homogeneous and isotropic with temperature-dependent properties; the thermoelectric properties such as electrical resistivity ρ , Seebeck coefficient α , and thermal conductivity κ are specified in polynomial functions of temperature (as given in Table 1 [15]); the thermal and electrical contact resistances at the interface of the thermoelectric and copper materials are neglected.

The system of partial differential equations governing the thermoelectric phenomenon in thermoelectric materials under steady-state conditions for the current flow continuity and heat transport [19] are written as:

$$\nabla \cdot \mathbf{J} = 0 \quad (1)$$

$$\nabla(\kappa \nabla T) + \rho \mathbf{J}^2 - \mathbf{T} \cdot \left[(\nabla \alpha)_T + \left(\frac{\partial \alpha}{\partial T} \right) \nabla T \right] = 0. \quad (2)$$

In Eq. (2), the second, third and fourth terms on the left-hand side of the second equation represent the Joule heating, Peltier and Thomson effects, respectively. Although the Thomson effect is not of primary importance as compared to Joule and Peltier effects

Table 1
Grid independence study for composite and conventional thermoelectric devices (grid size in bold face is chosen for further simulations).

Cells	P_0 W	% of error $\frac{ P_{0\text{new}} - P_{0\text{old}} }{P_{0\text{new}}} \times 100$	Q_h W	% of error $\frac{ Q_{h\text{new}} - Q_{h\text{old}} }{Q_{h\text{new}}} \times 100$	η %	% of error $\frac{ \eta_{\text{new}} - \eta_{\text{old}} }{\eta_{\text{new}}} \times 100$
Composite TED [at $T_h = 550$ K, $T_c = T_{\text{atm}} = T_{\text{sur}} = 300$ K, $d = 1$ mm, $H = 10$ mm, $h = 20$ W/m ² K and $R_L = 1.0 \times 10^{-3}$ Ω]						
11,6928	0.6856		13.2015		5.1930	
208,568	0.6843	0.1802	13.2492	0.3604	5.1650	0.5426
444,800	0.6831	0.1823	13.2357	0.1022	5.1608	0.0800
877,500	0.6815	0.2235	13.2105	0.1908	5.1591	0.0326
Conventional TED [at $T_h = 550$ K, $T_c = T_{\text{atm}} = T_{\text{sur}} = 300$ K, $H = 10$ mm, $h = 20$ W/m ² K and $R_L = 1.15 \times 10^{-2}$ Ω]						
102,076	0.2007		3.4341		5.8443	
204,732	0.2008	0.0486	3.4371	0.0890	5.8420	0.5426
393,600	0.2007	0.0429	3.4360	0.0318	5.8413	0.0800
528,640	0.2007	0.0082	3.4362	0.0033	5.8407	0.0326

Table 2Comparison of thermoelectric generator parameters $T_h = 427^\circ\text{C}$ and $T_c = 27^\circ\text{C}$.

Quantity	Analytical [21]	ANSYS (a) [22]	ANSYS (b) [22]	Present (a)	Present (b)
Q_h, W	13.04	13.03	11.07	13.0	10.72
P_o, W	1.44	1.43	1.05	1.43	1.07
$\eta(P_o/Q_h), \%$	11	11	9.5	11	9.98
I, A	19.2	19.1	16.4	19.09	16.5

in thermoelectric devices, it has been considered for completeness of analysis. The governing equation for heat transport in the connectors and inter-connectors can be obtained from Eq. (2) by merely removing the Peltier and Thomson effects.

Using the non-Ohmic current–voltage [20] relationship, the total electric potential is calculated as:

$$\nabla V = \nabla V_0 + \nabla V_S = -\rho J - \alpha \nabla T. \quad (3)$$

The first term on the right-hand side of Eq. (3) is the electrostatic potential distribution due to produced electric current and the second term represents the electric potential distribution from the Seebeck effect via the temperature gradient within the thermoelectric material. Since the temperature distribution and current density are three-dimensional (3D), one would expect the voltage distribution to be 3D as well.

The associated thermal and electrical boundary conditions for Eqs. (1)–(3) with respect to the geometry as shown in Fig. 1 are as follows.

At the ‘in’ terminal:

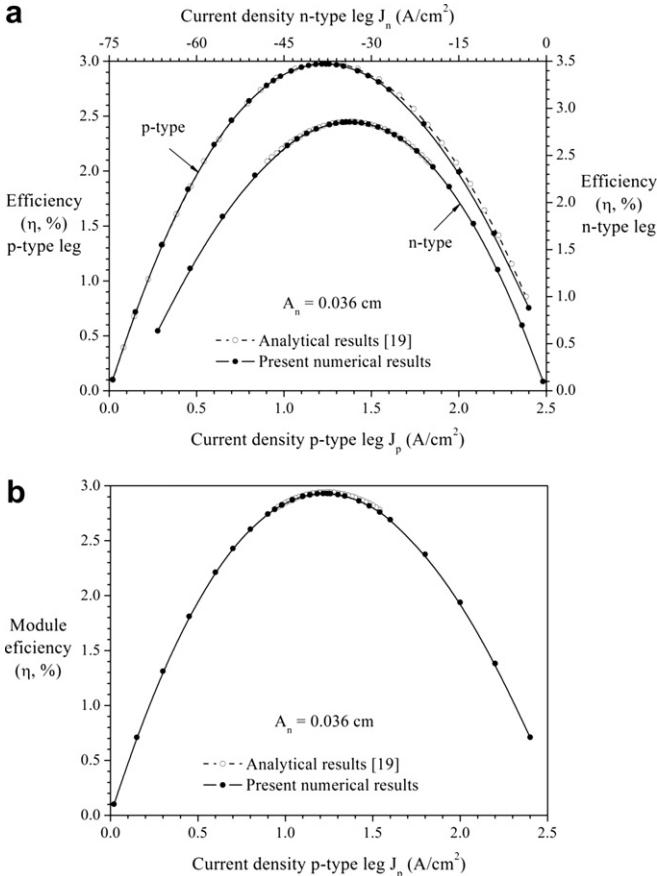


Fig. 2. Comparison of efficiencies for example 1 in Ref. [19] (a) efficiency of n-type and p-type legs (b) module efficiency of p-type leg.

$$J = \frac{I}{A_\xi} = \frac{V_0}{A_\xi(R_i + R_L)} \quad \text{and} \quad \frac{\partial T}{\partial \xi} = 0, \quad (4)$$

where V_0 is the Seebeck voltage. The Seebeck voltage is the open circuit voltage produced when a temperature differential is imposed across the junctions of the device at a no load condition. Furthermore, V_0 is the summation of the Seebeck potentials at the interfaces of the semiconductor and conductor materials and is expressed as

$$V_0 = \sum_{j=n,p} \sum_{i=1}^2 \frac{L_{ji}}{A_{Sji}} \int_{A_{Sji}} |\alpha_{ji}| \frac{dT}{d\xi} dA_{Sji}. \quad (5)$$

The above Seebeck potentials, with reference to the hot side temperature, are evaluated at the cold side of the interface of the semiconductor and inter-connector materials.

In Eq. (4), R_i and R_L are the total internal and external load resistances, respectively. The R_i of the CTED is evaluated as

$$R_i = \sum_{i=n,p,c,lc} \frac{L_i}{A_i} \left[\frac{1}{V_i} \int_{V_i} \rho_i dv_i \right], \quad (6)$$

where V is the volume of the material.

At the ‘out’ terminal:

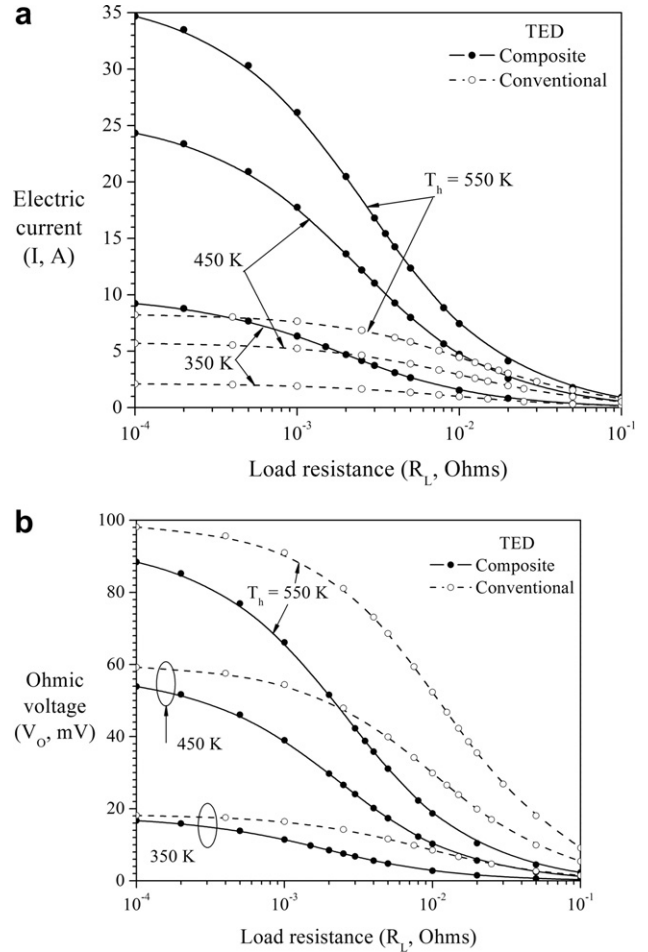


Fig. 3. Effects of load resistance on (a) electrical current and (b) Ohmic voltage for various hot wall temperature T_h values [at $d = 1 \text{ mm}$, $h = 20 \text{ W m}^{-2} \text{ K}^{-1}$, $T_c = T_\infty = T_{\text{sur}} = 300 \text{ K}$].

$$V = 0 \quad \text{and} \quad \frac{\partial T}{\partial \xi} = 0. \quad (7)$$

At the top wall of the upper connector:

$$T = T_h \quad \text{and} \quad \frac{\partial V}{\partial \xi} = 0. \quad (8)$$

At the bottom wall of the lower connector:

$$T = T_c \quad \text{and} \quad \frac{\partial V}{\partial \xi} = 0. \quad (9)$$

At all other surfaces exposed to surroundings:

$$q'' = h(T - T_\infty) + \epsilon\sigma(T^4 - T_{\text{sur}}^4). \quad (10)$$

Here, in Eq. (10), the first and the second terms on the right hand side represent the effects of convection heat transfer and radiation on TED, respectively. The emissivities ϵ for the semiconductor and the highly polished copper conductor are taken as 0.45 and 0.03, respectively. The ambient fluid (T_∞) and the surrounding (T_{sur}) temperatures are kept constant.

At the interface between the semiconductor and conductor materials, the continuity of temperature, current density and the heat flux conditions are imposed and are written as

$$T_{c,\text{ic}} = T_{n,p}, \quad J_{c,\text{ic}} = J_{n,p}, \quad \text{and} \quad -\frac{dT_{c,\text{ic}}}{d\xi} = -\frac{\kappa_{n,p}}{\kappa_{c,\text{ic}}} \frac{dT_{n,p}}{d\xi}, \quad (11)$$

where ξ denotes the direction normal to the corresponding wall of the element.

The power output from the TED for a given load resistance R_L and heat input at the hot wall are evaluated as

$$P_0 = I^2 R_L, \quad Q_h = -\int \kappa_c \frac{\partial T}{\partial \xi} dA_s \quad (12)$$

and the thermal conversion efficiency is calculated as

$$\eta = \frac{P_0}{Q_h}. \quad (13)$$

3. Numerical solution procedure and validation

The numerical simulations are performed in a FLUENT-UDS (User Defined Scalar) environment using the finite volume formulation of the governing Eqs. (1) and (2), and the constitutive relation (Eq. (3)) along with the associated boundary conditions (Eqs. (4) and (7)). FLUENT has well-implemented fluid and heat transfer models, allowing us to numerically investigate the thermo-fluid-electrical coupling mechanisms in TEDs. Additionally, numerical solutions for a thermoelectric generator have been demonstrated using the UDS package in FLUENT [13].

The geometric models and mesh are generated in Gambit 2.4. The Ohmic heating, Peltier and Thomson effects are modeled as source terms in the energy equation (Eq. (2)). The Ohmic and

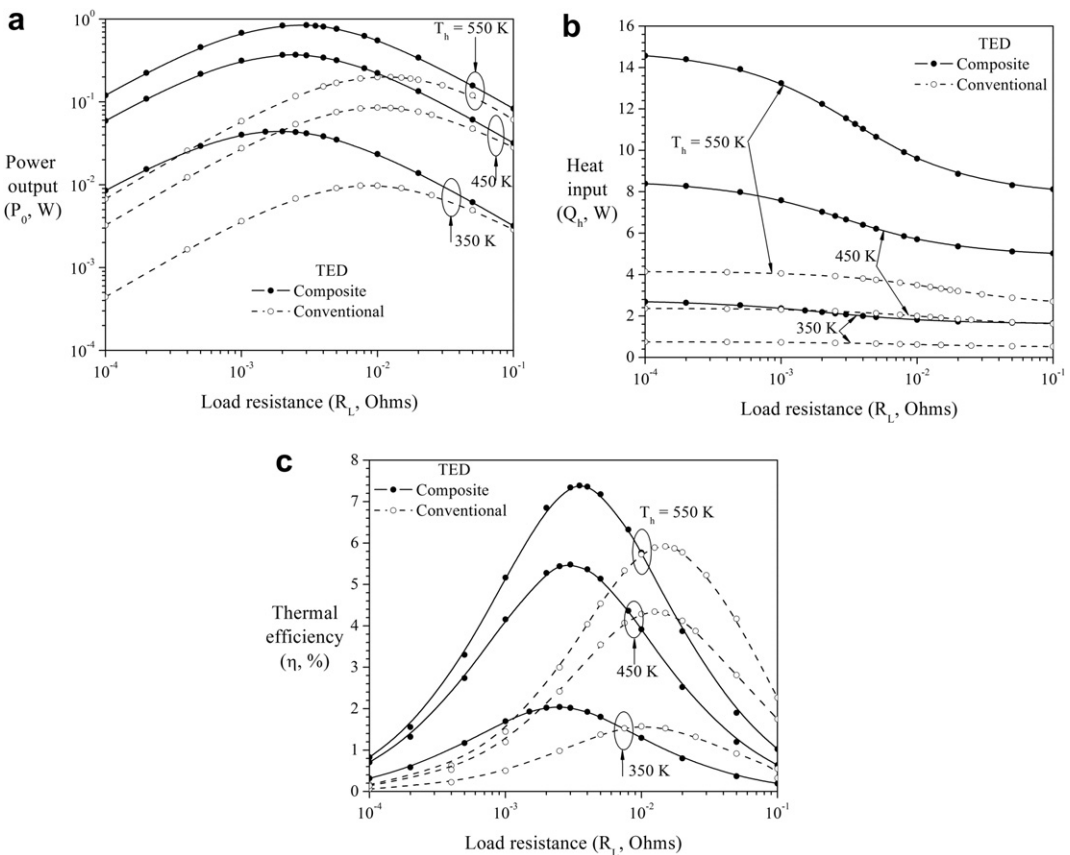


Fig. 4. Effects of load resistance on (a) electrical power output (b) heat input and (c) thermal efficiency for various hot wall temperature T_h values [at $d = 1$ mm, $h = 20 \text{ W m}^{-2} \text{ K}^{-1}$, $T_c = T_\infty = T_{\text{sur}} = 300 \text{ K}$].

Seebeck potential distributions (Eq. (3)) are calculated using UDS fields. The spatial discretization of the diffusion term is done with a power law scheme. For a given load resistance R_L , the electric current (as expressed in (Eq. (4))) is evaluated based on the open-circuit Seebeck voltage (Eq. (5)) generated via the temperature differential applied at hot and cold junctions.

The convergence criteria (the absolute residual difference between consecutive iterations over a domain) for Ohmic and Seebeck potentials, and energy are set as 10^{-10} and 10^{-12} , respectively. Grid independence tests are performed for both composite and conventional TEDs (as shown in Fig. 1) and are depicted in Table 1. Grid sizes with 208,568 and 204,732 cells are

chosen for the analysis of composite and conventional TEDs, respectively. The orthogonal and non-uniform grid is employed for succinctness and the computational mesh used for simulations is shown in Fig. 1.

The three-dimensional thermoelectric model has been validated with published results of a thermoelectric generator for the cases of (a) constant properties [21] and (b) temperature-dependent properties [22] as given in Table 2. Fig. 2 also depicts the validation of the present numerical code with one of the examples from [19] in terms of individual leg and module efficiencies. The results are in good agreement with published analytical and numerical results.

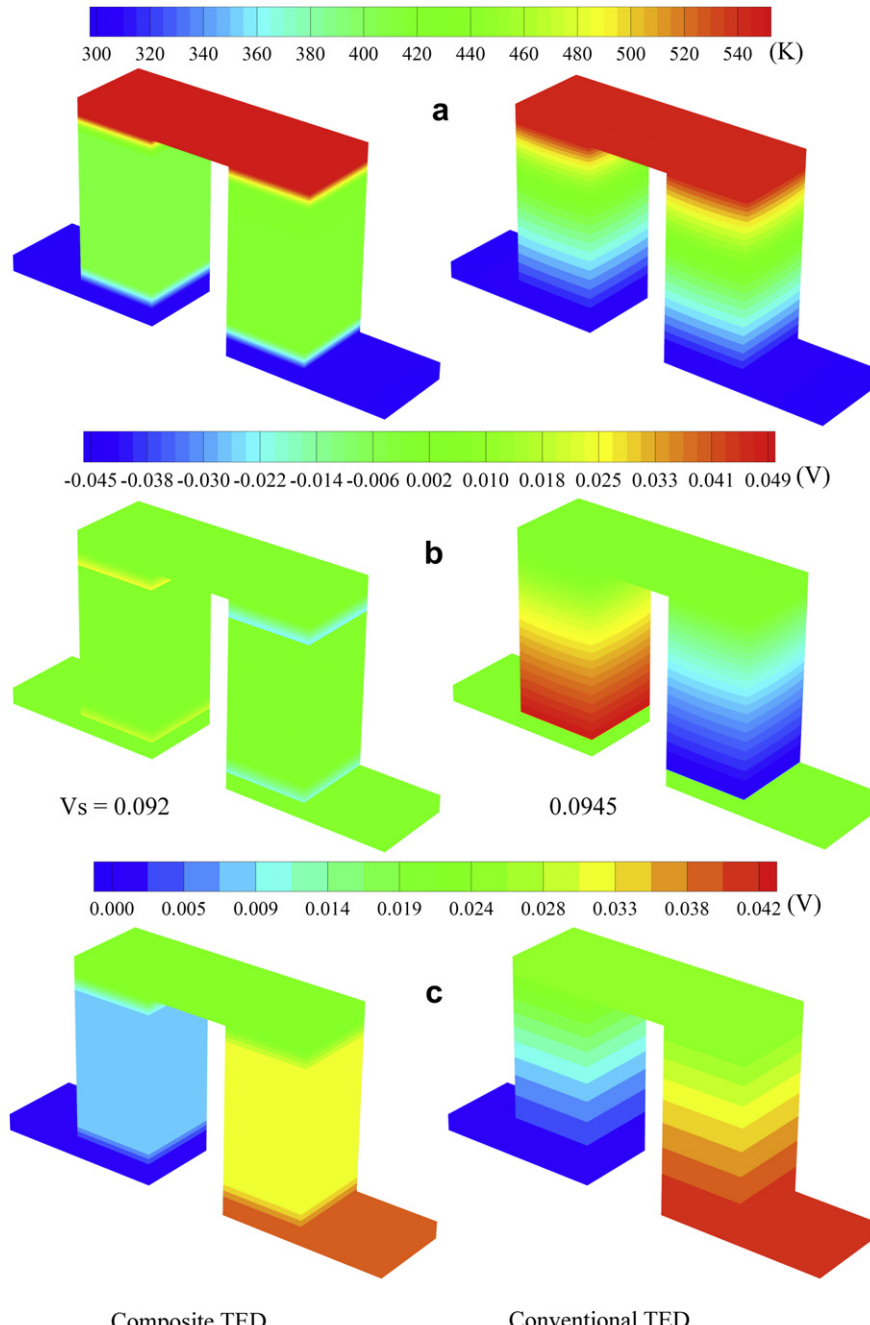


Fig. 5. The contours of (a) temperature (b) Seebeck and (c) Ohmic voltages at optimum load resistance values for both composite and conventional TEDs [$T_h = 550$ K, $d = 1$ mm, $h = 20 \text{ W m}^{-2} \text{ K}^{-1}$, $T_c = T_\infty = T_{\text{sur}} = 300$ K].

4. Results and discussion

The numerical simulations are conducted on composite thermoelectric devices (CTEDs) as well as a convectional TED made with n-type (75% Bi₂Te 25% Bi₂Se), p-type (25% Bi₂Te₃ 75% Sb₂Te₃ (1.75% excess Se)), and copper materials. The connector has a geometry of length by depth by height of 35 × 5 × 1 mm³. The height of the thermoelectric leg is $H = 10$ mm and the cross-sectional area of the n- or p-type leg is 5 × 5 mm². The distance between the legs is $L_2 = 5$ mm. The cold wall, ambient and surrounding temperatures ($T_c = T_\infty = T_{\text{sur}} = 300$ K), and the geometric dimensions as given above are invariant in the present study. The influence of the hot wall temperature $350 \leq T_h$ (K) ≤ 550, the load resistance $10^{-4} \leq R_L (\Omega) \leq 10^{-1}$, the semiconductor thickness $0.25 \leq d (\text{mm}) \leq 4$ and the convection heat transfer coefficient $0 \leq h (\text{W m}^{-1} \text{K}^{-1}) \leq 10^3$ on the thermo-electric performance of a CTED compared with geometrically equivalent conventional TED's values has been investigated in detail.

Considering a geometrically equivalent CTED with $d = 1$ mm and a conventional TED for a given $h = 20 \text{ W m}^{-1} \text{K}^{-1}$ value, Fig. 3 shows the variation of the electric current I and the Ohmic voltage drop V_0 while Fig. 4 depicts the heat input Q_h , power output P_0 and the thermal conversion efficiency η with respect to load resistance R_L for different values of hot wall temperatures T_h . In these figures, the solid lines with filled circles represent the results for a CTED and the dotted lines with empty circles describe conventional TED values. From Figs. 3 and 4, it is observed that for a given R_L value, an increase in T_h results in an increase in I , V_0 , P_0 , Q_h and η values. However, at a given T_h , an increase in R_L decreases both I and V_0 values, with these values eventually approaching zero at larger R_L value. This indicates the TED produces zero P_0 at large R_L value even though the device experiences a temperature differential $T_h - T_c$. The similar behavior is also observed in the conventional TED. For a given R_L , the CTED's I value is higher as compared to the conventional TED. On the other hand, the opposite behavior is observed for V_0 . This is due to the total internal resistance R_i (summation of copper and semiconductor materials, i.e. $R_c + R_n + R_p$) of the CTED being less as compared to the conventional TED. It is noticed that the difference between the ordinate values of the CTED and the conventional TED decreases with R_L in case of I , whereas the similar behavior has not been seen for V_0 . Moreover, when $R_L < 2 \times 10^{-2}$, there is a substantial change in I and V_0 values.

In Fig. 4a and c, for a given T_h , it is observed that there exists a maximum P_0 when $R_L = R_i$ and an optimum η at a particular resistance R_L known as the optimum load resistance R_{optml} . For the CTED, the R_i values (in Ω, as calculated from Eq. (6)) evaluated at $T_h = 350, 450$ and 550 K are $1.855 \times 10^{-3}, 2.217 \times 10^{-3}$, and 2.254×10^{-3} , respectively; for the conventional TED, the values are $8.645 \times 10^{-3}, 9.991 \times 10^{-3}$, and 1.1135×10^{-2} . The R_{optml} increases with an increase in T_h values while all other parameters are kept constant. The R_{optml} values for the CTED are one order of magnitude less than the conventional TED, and interestingly enough, the CTED's behavior is extremely similar to that of the conventional TED. However, greater P_0 values and lesser R_{optml} values are predicted for the CTED when compared to the conventional TED. It is also observed that the optimum η values of the CTED are 24.8%, 26.2% and 29.9% higher than the conventional TED at $T_h = 550$ K, 450 K and 350 K, respectively. This trend is due to P_0 and Q_h being functions of R_i ; as R_i decreases for the same T_h value, Q_h increases, and the inverse is true; Q_h decreases with an increase in R_i value. Moreover, within the specified R_L range, the CTED is subjected to higher T_h values and shows a dramatic change in Q_h predictions. As shown Fig. 4b, the CTED exhibits

nearly a three-fold increase in Q_h values when compared to the conventional TED.

For a given $T_h = 550$ K and $h = 20 \text{ W m}^{-1} \text{K}^{-1}$, the three-dimensional (3D) distributions of temperatures, Seebeck and Ohmic potentials for both composite ($d = 1$ mm) and conventional TEDs are plotted in Fig. 5. Here, the R_L is taken at the optimum η value (Fig. 4) for the corresponding TED case. For a given $T_h - T_c$, irrespective of the TED case, the temperature has to flow from the hot side surface to the cold side surface. It is observed that the temperature and voltage gradients in the semiconductor material of the CTED are higher compared to the conventional TED. It is also observed that the temperature and Ohmic voltage gradients are negligible in the conductor material as compared to the semiconductor material. This is attributed to the high thermal and electrical conductivity of the conductor material. It can be seen that the presence of lower a convection heat transfer coefficient results in minimal nonconformity in the temperature and voltage distributions of leg. Due to larger R_i of the conventional TED, the Ohmic voltage drop and the total built-in Seebeck voltage values are higher when compared to the CTED values.

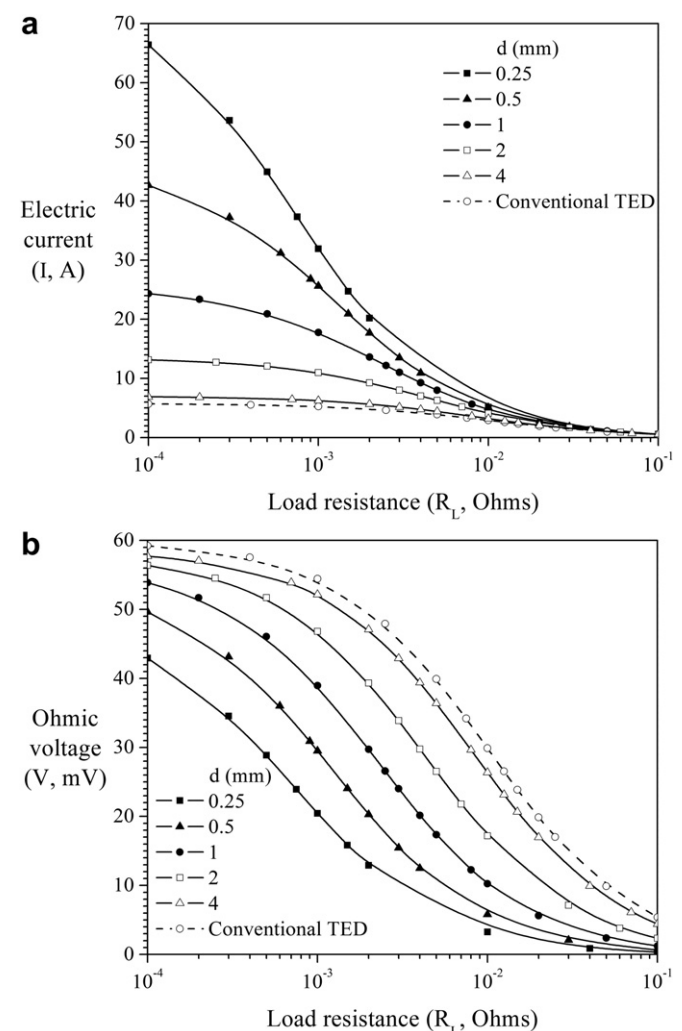


Fig. 6. The variation of (a) electrical current and (b) Ohmic voltage with load resistance for different semiconductor thickness d values [at $T_h = 450$ K, $h = 20 \text{ W m}^{-2} \text{K}^{-1}$, $T_c = T_\infty = T_{\text{sur}} = 300$ K].

Figs. 6 and 7 show the electrical and thermal characteristics (I , V_0 , P_0 , Q_h , and η) of a CTED for different semiconductor thickness d and load resistance R_L values with conditions of $T_h = 450$ K and $h = 20 \text{ W m}^{-2} \text{ K}^{-1}$. The CTED qualitatively shows similar behavior for a given d value as illustrated in Figs. 4 and 5. Furthermore, for a specified R_L value, an increase in d results in a decrease in I and an increase in V_0 . There is a significant change in I when $R_L < 2 \times 10^{-3}$; however, a moderate change in V_0 for the range $10^{-4} \leq R_L \leq 10^{-1}$ is observed. This behavior is explained by the cumulative effect of R_i and R_L on I for a given $T_h - T_c$ value. For instance, the contours of the Seebeck V_S and Ohmic V_0 potentials for various d values at R_{optmL} are shown in Fig. 8. The percentage change in the total absolute value of V_S (as depicted in Fig. 8) is minimal with d when compared to the change in V_0 values. This is due to the temperature-dependence of the Seebeck coefficient and the minimal temperature drop across the inter-connector material.

From Fig. 7c, it is seen that as d increases the optimum η value increases, and it reaches a maximum value at $d = 1 \text{ mm}$. After that, the optimum η starts decreasing with an increase in d . Interestingly, the optimum η value of the conventional TED is higher than CTED case when $d = 4 \text{ mm}$. The interplay of geometric dimensions, heat loss to surroundings and the boundary conditions at the hot and cold surfaces explains the effect on the optimum η values. From Fig. 7a and c, both P_0 and Q_h substantially increase with a decrease in d values. Additionally, the R_{optmL} value increases with an increase in d . Irrespective of the d value, beyond $R_L = 10^{-1}$, the P_0 reaches a single value which represents the conventional TED value (as shown in Fig. 7a). The Q_h as seen in Fig. 7b shows a higher value at

$d = 0.25 \text{ mm}$ for a given R_L value as compared to other d values. Moreover, as semiconductor thickness d doubles, heat input Q_h approximately reduces to half value and vice-versa. This increase in Q_h with reduction in d is due to the rise in the effective thermal conductance of the leg while maintaining a fixed $T_h - T_c$ value. The temperature distribution in the CTED for different d values is depicted in Fig. 8. It is noticed that the temperature gradients in the semiconductor increases with a decrease in d and vice-versa. From Fig. 8, it is also observed that at a given h value, as d increases, the distributions of temperature and voltages become more three-dimensional.

For different values of d and T_h , the effects of the convection heat transfer coefficient h (represents the heat loss from the surfaces exposed to the surroundings) on the thermoelectric characteristics of the CTED are shown in Figs. 9 and 10. Here, in the simulations, the R_L is set equal to R_i (as depicted in Fig. 9c). For given d and T_h values, the variations in I , V_0 , and P_0 are negligible with an increase in h from 5 to 100; however, when $h > 100$, a noticeable change is observed in these values. Contrary to this trend, Fig. 10b and c illustrate a significant change in Q_h and η values for the same range of h values. In order to maintain the constant $T_h - T_c$ condition, the Q_h value is substantially increased, and hence η is reduced with an increase in h value. It is also observed that the influence of h on R_i is strong at higher T_h values as shown in Fig. 9c. For brevity, when $h = 0$ (no heat loss) condition, the performance parameter (I , V_0 , R_i , P_0 , Q_h , and η) values are given in these figures for the corresponding d and T_h values.

To put these findings into perspective of practical application, a simple cost analysis is presented. The percent reduction of

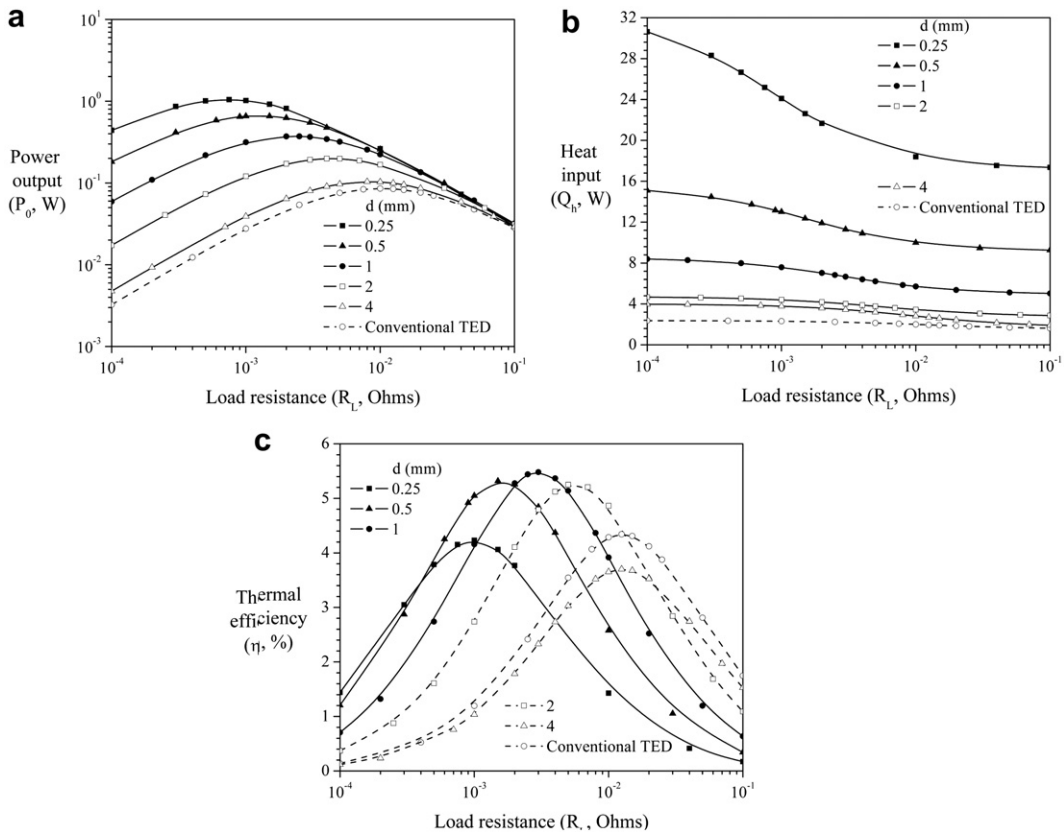


Fig. 7. The variation of (a) electrical power output (b) heat input and (c) thermal efficiency with load resistance for different semiconductor thickness d values [at $T_h = 450$ K, $h = 20 \text{ W m}^{-2} \text{ K}^{-1}$, $T_c = T_\infty = T_{\text{sur}} = 300$ K].

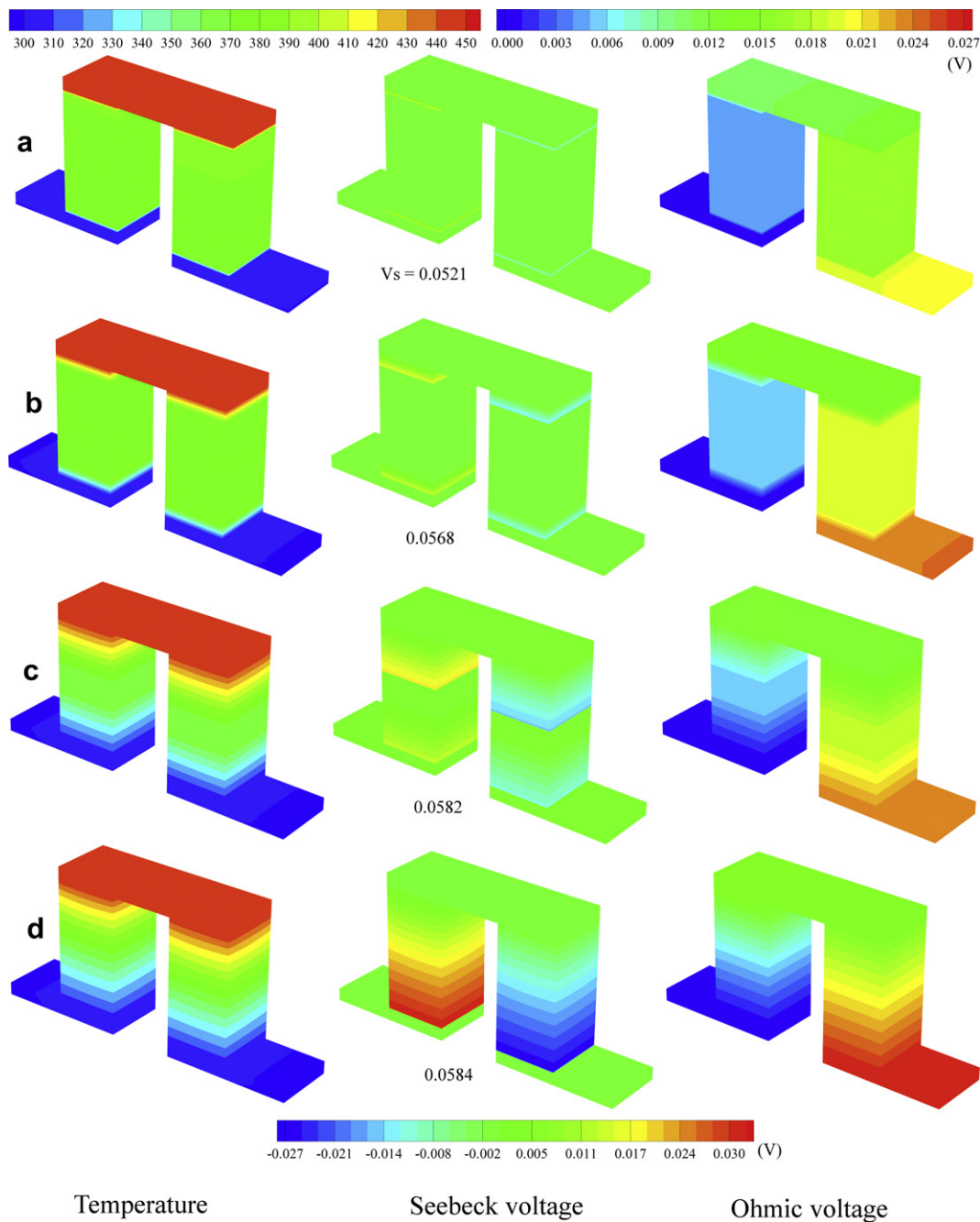


Fig. 8. The distributions of temperature, Seebeck and Ohmic voltages for different semiconductor thickness d (mm) (a) 0.25 (b) 1 (c) 4 and (d) 5 (conventional TED) at optimum load resistance values [at $T_h = 450$ K, $h = 20 \text{ W m}^{-2} \text{ K}^{-1}$, $T_c = T_\infty = T_{\text{sur}} = 300$ K].

material usage and associated costs of a composite leg are compared to a conventional leg as shown in Table 3. Based upon laboratory experiments, the price of commercially available bismuth–telluride semiconducting material is approximately \$0.72 per mm³. The corresponding high thermal conductivity oxygen free copper materials cost \$0.0069 per mm³. For instance, the cost of a composite leg (Fig. 1a) with $d = 0.5$ mm, $L = 10$ mm and a cross-section of 5 mm × 5 mm, (includes thermoelectric material and inter-connector) would be \$19.55, as compared to the conventional element with a cost of \$180. This reflects a rare-earth element material usage reduction of 90% and a cost reduction of

89.14%. Although the cost and rare-earth element material usage is reduced, this data does not reflect the extra processing needed to construct the composite leg: polishing of the copper surfaces which will be in contact with the bismuth–telluride; the nickel coating of the copper to prevent oxidation and rapid copper diffusion into the bismuth–telluride; the diffusion barrier deposition on top of the nickel coating to ensure prevention of nickel and copper diffusion into the semiconductor; the diffusion bonding process itself. All of these additional manufacturing steps do not have a quantifiable cost associated with the production of the composite leg.

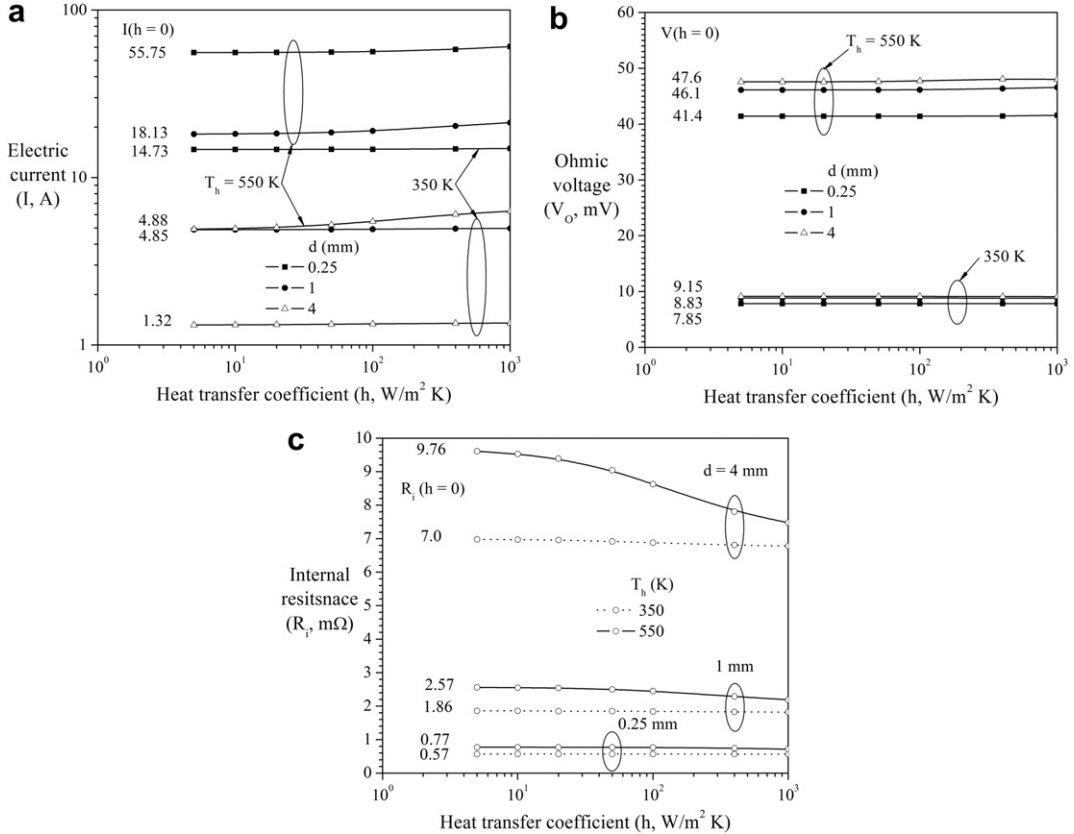


Fig. 9. The influence of convection heat transfer coefficient on (a) electrical current (b) Ohmic voltage and (c) internal resistance for various hot wall temperature T_h and semiconductor thickness d values [at $R_L = R_i$, $T_c = T_\infty = T_{\text{sur}} = 300$ K].

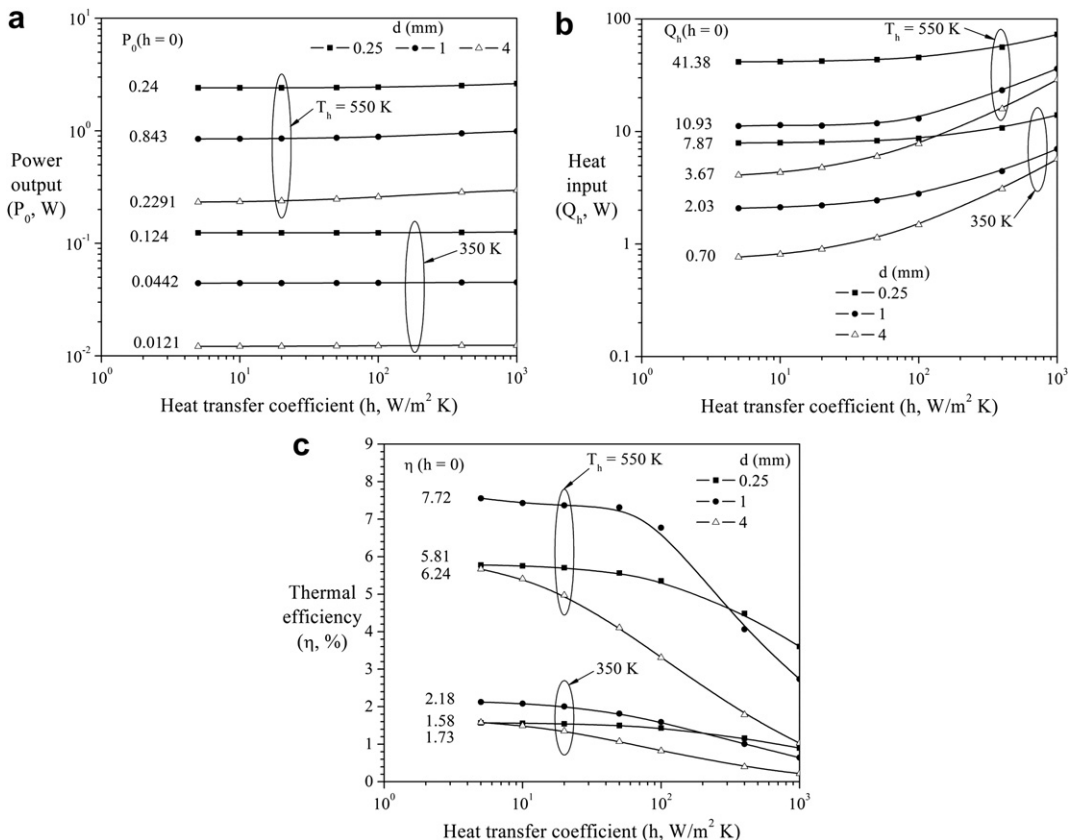


Fig. 10. The influence of convection heat transfer coefficient h on (a) electrical power output (b) heat input and (c) thermal efficiency for various hot wall temperature T_h and semiconductor thickness d values [at $R_L = R_i$, $T_c = T_\infty = T_{\text{sur}} = 300$ K].

Table 3

Quantitative comparison of composite leg material cost and usage with conventional leg ($H = 10$ mm, $W = 5$ mm and $D = 5$ mm).

Semiconductor element size (d , mm)	Cost of composite leg (in US dollars)	% of reduction in material cost	% of reduction in material usage
0.25	10.64	94.09	95
0.5	19.55	89.14	90
1	37.38	79.23	80
2	73.04	59.43	60
4	144.35	19.81	20

5. Conclusions

Using the FLUENT-UDS environment, the thermoelectric coupling mechanisms of Joule heating, Peltier cooling, and Thomson cooling/heating in a thermoelectric material with temperature-dependent properties have been implemented. Oriented toward improving a thermoelectric device's (TED) power output and also minimizing the usage of rare-earth materials (n or p-type) in waste heat recovery applications, a novel composite thermoelectric device (CTED) has been proposed without compromising its thermal conversion efficiency.

The thermoelectric performance of a CTED compared with a conventional TED in terms of electric current I , Ohmic V_O and Seebeck V_S voltages, power output P_0 , heat input Q_h and thermal conversion efficiency η for different values of hot surface temperature T_h , load resistance R_L , semiconductor thickness d , and convection heat transfer coefficient h are investigated in detailed using numerical simulations.

The difference in power outputs of composite and conventional TEDs is decreased with an increase in R_L while all other parameters are kept constant. It is demonstrated that P_0 reaches a maximum at R_L equaling the total internal resistance R_i and η attains an optimum at an optimum load resistance R_{optml} . For the CTED, the R_{optml} is lower than the conventional TED value. For both TEDs, a marginal increase in R_{optml} value with an increment in T_h is noticed. It is also observed that a CTED with $d = 1$ mm shows a 24.8%, 26.2%, and 29.9% increase in η as compared to a geometrically equivalent conventional TED when $T_h = 550$ K, 450 K and 350 K, respectively. At the minimum stated temperature, the CTED showed a near three-fold increase in Q_h .

For the CTED, it is noticed that as d increases the optimum η value increases, and it reaches a maximum value at $d = 1$ mm. After that, the optimum η starts declining with an increase in d . On the other hand, both P_0 and Q_h substantially increase with a reduction in the d value. At higher R_L values, irrespective of the d value, the P_0 value reaches that of a conventional TED. Moreover, as d is reduced by half, the Q_h approximately doubles.

For a given CTED configuration d and temperature differential $T_h - T_c$, the convection heat transfer coefficient h has a negligible effect on P_0 . However, h has a marginal influence on both Q_h and η values.

Finally, it is proposed that building state-of-the-art novel CTEDs with a minimum amount of rare-earth metals reduces cost without compromising thermal conversion efficiencies and performance,

greatly helping with the production of clean energy from waste heat resources.

References

- [1] D. Rowe, Thermoelectric waste heat recovery as a renewable energy source, *International Journal of Innovations in Energy Systems and Power* 1 (1) (2006) 13–23.
- [2] B. Poudel, M.Y. Hao, Q.Y. Lan, A. Minnich, B. Yu, X. Yan, D. Wang, A. Muto, D. Vashaee, X. Chen, J. Liu, M.S. Dresselhaus, G. Chen, Z. Ren, High-thermoelectric performance of nanostructured bismuth antimony telluride bulk alloys, *Science* 320 (5876) (2008) 634–638.
- [3] T.M. Tritt, Thermoelectric phenomena, materials, and applications, *The Annual Review of Materials Research* 41 (2011) 433–448.
- [4] T. Caillat, J.P. Fleuriot, G.J. Snyder, A. Zoltan, D. Zoltan, A. Borshchevsky, Development of a high efficiency thermoelectric unicouple for power generation applications, in: *Proceedings of the XVIII International Conference on Thermoelectrics*, Baltimore, USA, 1999.
- [5] X. Gou, H. Xiao, S. Yang, Modeling, experimental study and optimization on low-temperature waste heat thermoelectric generator system, *Applied Energy* 87 (2010) 3131–3136.
- [6] Y. Hsiao, W. Chang, S. Chen, A mathematic model of thermoelectric module with applications on waste heat recovery from automobile engine, *Energy* 35 (2010) 1447–1454.
- [7] R. Harris, T. Hogan, H.J. Schock, T.I.-P. Shih, Heat transfer and electric current flow in a thermoelectric couple, in: *44th Aerospace Sciences Meeting and Exhibition*, 575, AIAA, Reno, Nevada, 2006.
- [8] M. Chen, L.A. Rosendahl, T.J. Condra, J.K. Pedersen, Numerical modeling of thermoelectric generators with varying material properties in a circuit simulator, *IEEE Transactions on Energy Conversion* 24 (1) (2009) 112–124.
- [9] K.S.-Y. Hu, Heat Transfer Enhancement in Thermoelectric Power Generation, M.S. Iowa State University, 2009.
- [10] P. Ziolkowski, P. Poinas, J. Leszczynski, G. Karpinski, E. Muller, Estimation of thermoelectric generator performance by finite element modeling, *Journal of Electronic Materials* 39 (9) (2010) 1934–1943.
- [11] T. Kousksou, J.-P. Bdcarrats, D. Champier, P. Pignolet, C. Brillet, Numerical study of thermoelectric power generation for an helicopter conical nozzle, *Journal of Power Sources* 196 (2011) 4026–4032.
- [12] C.A. Gould, N.Y.A. Shammas, S. Grainger, I. Taylor, A novel 3D TCAD simulation of a thermoelectric couple configured for thermoelectric power generation, in: *International Conference on Renewable Energies and Power Quality*, Spain (2011).
- [13] M. Chen, L.A. Rosendahl, T. Condra, A three-dimensional numerical model of thermoelectric generators in fluid power systems, *International Journal of Heat and Mass Transfer* 54 (2011) 345–355.
- [14] M.K. Chyu, B.V.K. Reddy, M. Barry, J. Li, Enhanced heat transfer characteristics and performance of composite thermoelectric devices, in: *International Conference on Advanced Computational Methods and Experiments in Heat Transfer XII*, vol. 35, WIT Press, Split, Croatia, 2012, pp. 13–24.
- [15] B.V.K. Reddy, M. Barry, J. Li, M.K. Chyu, Three-dimensional multiphysics coupled field analysis of an integrated thermoelectric device, *Numerical Heat Transfer Part A* 62 (2012) 933–947.
- [16] B.V.K. Reddy, M. Barry, J. Li, M.K. Chyu, Thermoelectric performance of novel composite and integrated devices applied to waste heat recovery, *ASME Journal of Heat Transfer*, in press, 12.
- [17] M. Hodes, Optimal pellet geometries for thermoelectric power generation, *IEEE Transactions on Components and Packaging Technologies* 33 (2010) 307–318.
- [18] B. Jan, S. Han, J.-Y. Kim, Optimal design for micro-thermoelectric generators using finite element analysis, *Microelectronic Engineering* 88 (2011) 775–778.
- [19] T.P. Hogan, T. Shih, *Thermoelectrics Handbook Macro to Nano*, CRC Press, Taylor & Francis Group, Boca Raton, 2006 (Chapter 12).
- [20] C.A. Domenicali, Stationary temperature distribution in an electrically heated conductor, *Journal of Applied Physics* 25 (1954) 1310–1311.
- [21] S.W. Angrist, *Direct Energy Conversion*, fourth ed., Allyn and Bacon Inc., Boston, 1982.
- [22] E.E. Antonova, D.C. Looman, Finite elements for thermoelectric device analysis in ANSYS, in: *IEEE International Conference on Thermoelectrics*, 2005, pp. 200–203.